Ferroelectric transition under hydrostatic pressure in poly(vinylidene fluoride–trifluoroethylene) copolymers

E. Bellet-Amalric* and J. F. Legrand
Institut Laue–Langevin, BP 156X, 38042 Grenoble Cedex, France

and M. Stock-Schweyer and B. Meurer
Institut C. Sadron, 6 rue Boussingault, 67083 Strasbourg Cedex, France
(Received 18 January 1993; revised 29 March 1993)

A clear ferroelectric transition of first-order type is observed in poly(vinylidene fluoride–trifluoroethylene) (P(VDF–TrFE)) random copolymers with TrFE contents higher than 20% and lower than 40%. This structural phase transition which takes place in the crystalline regions of the polymeric material has been analysed using neutron diffraction under hydrostatic pressure for three copolymer compositions: 80/20, 70/30 and 60/40. The P–T phase diagrams have been determined in the ranges 0.1–300 MPa, 300–500 K both upon heating and upon cooling, and several thermodynamic parameters have been evaluated for the different crystalline phases: compressibility and thermal expansion coefficients, enthalpies of transition, etc. For the middle composition (70/30) the ferroelectric transition temperature T_C is well separated from the melting temperature T_m of the paraelectric phase and both transition temperatures increase with increasing pressure: $dT_C/dP = 0.38\ K\ MPa^{-1}$ and $dT_m/dP = 0.25\ K\ MPa^{-1}$. For the 80/20 composition the Curie temperature T_C is closer to the melting temperature T_m, and under increasing pressure the two transition lines are expected to merge at a triple point ($P^* \approx 500$ MPa, $T^* \approx 560$ K), above which a single line corresponds to the melting of the ferroelectric phase. For the 60/40 composition a new 'low temperature disordered' phase appears and coexists with the ferroelectric phase but with a volume fraction which depends on temperature and thermal history.

(Keywords: VDF–TrFE copolymers; semi-crystalline polymers; ferroelectric phase transition)

INTRODUCTION

Among the few ferroelectric polymers known at present, copolymers of vinylidene fluoride (VDF) and trifluoroethylene (TrFE) have attracted much scientific and technological research because of their piezoelectric and pyroelectric effects[1].

In these materials, the crystalline lamellae, which represent more than 60% of the volume, are embedded in an amorphous matrix and this feature confers to the polymeric material a 'composite' microstructure[2,3].

As with other ferroelectric crystals these copolymers exhibit a ferroelectric–paraelectric transition which has been clearly observed for VDF contents ranging from 65 to 80%[4,5].

In these copolymers the ferroelectric transition temperature is strongly dependent upon the dipolar energy which is responsible for the stability of the ferroelectric order and which decreases both with the VDF content[6] and after electron or γ-ray irradiation[7]. The characteristics of these copolymers are also very sensitive to thermal treatments[3], mechanical orientation and electrical poling[2], which affect the microstructure and the degree of crystallinity.

For less than 65% VDF content, the structure of the low temperature phase is not completely understood: Lovinger *et al.*[4] have reported the coexistence of a ferroelectric phase with a disordered helical phase; alternatively, Tashiro *et al.*[5] have proposed an intermediate phase called the 'cooled phase' consisting of a kind of micro-twinning of the small ferroelectric crystals.

The effects of hydrostatic pressure have already been studied by several methods, mainly in copolymers with VDF contents lower than 60%[8–12]. Most of these investigations have been performed on a macroscopic scale, e.g. dielectric measurements[10,11], differential thermal analysis[8] and ferroelectric hysteresis curves[9], thus mixing the contributions of the amorphous and crystalline regions. Only a few studies, based on X-ray diffraction[8,12], provide information on the crystalline phases.

The present work was undertaken in order to analyse the thermodynamic properties of the ferroelectric and paraelectric crystalline phases under hydrostatic pressure for different contents of VDF. Neutron diffraction experiments permit the use of heavy vessels like high pressure cells, cryostats, etc. and are therefore well suited for the determination of phase diagrams and for studies of the evolution of the lattice parameters *versus* temperature and pressure. These allow the determination of the compressibility and the thermal expansion of the crystalline phases and the volume change of the unit cell through the ferroelectric transition.

* To whom correspondence should be addressed

0032-3861/94/010034-13
© 1994 Butterworth-Heinemann Ltd.

EXPERIMENTAL

Samples

The samples used in this study were random P(VDF–TrFE) copolymers of compositions 70/30, 80/20 and 60/40 mol% supplied by Atochem, France. From gel permeation chromatography (g.p.c.) all the samples had approximately the same molecular weight $\overline{M}_n \approx 100\,000$ and the same polydispersity index $\overline{M}_w/\overline{M}_n \approx 2$. Moreover, the microstructural data, obtained by high resolution n.m.r., confirmed the randomness of the monomer distribution[13].

The raw material was melted in a cylindrical vanadium container of 40 μm wall thickness almost transparent to neutrons (5 mm in diameter and 20 mm in length). Such a preparation is considered to have no effect on the orientation of the sample (isotropic powder symmetry maintained). For each composition all the measurements were carried out with the same specimen.

Before conducting the sequence of measurements a pressure cycle, up to 300 MPa and back to atmospheric pressure, and a temperature cycle, up to the paraelectric phase and back to room temperature, were carried out in order to remove any possible residual stress in the specimen.

Neutron diffraction instrument

The experiments were performed at the Institut Laue–Langevin on the high flux powder diffractometer D20. A graphite monochromator ((002) reflection) provided a neutron beam of wavelength 2.41 Å defined to within 0.01 Å. The precise wavelength and the angular position of the incident beam were calibrated using a silicon powder standard. The beam size and the resolution were determined by the natural divergence of the beam (10 mrad) and by diaphragms positioned between the monochromator and the sample (10 mm × 20 mm).

The instrument D20 is equipped with a multielectrode, position sensitive ^{3}He detector which covers an angular range of 12.6° (126 channels) and can be moved step by step around the sample axis to cover wider angular ranges. The channel sensitivities were calibrated with an isotropic incoherent scatterer (vanadium). In order to reduce parasitic scattering and to protect the detector from receiving the direct beam, additional cadmium screens and slits were positioned along the beam path.

Sample environment

The sample container was placed in a pressure vessel made of a copper–beryllium alloy which allows pressures of up to 300 MPa and temperatures of up to 500 K[14]. Helium gas was used for transmitting the pressure from the compressor to the sample chamber. The pressure was measured outside the vessel with a manganese gauge having an accuracy of about 2%.

The pressure cell was placed in a cryo-furnace (1.5–600 K) whose temperature regulation was ensured by an analog controller. The temperature of the pressure cell was measured using a rhodium–iron resistor.

Measurement procedures

The measurements were carried out in two different ways.

Isobaric temperature scans. These were performed with continuous slow heating and subsequent cooling. A rate of about 0.5 K min^{-1} was chosen in order to get a good temperature homogeneity and to avoid any kinetic effects[3]. The acquisition time of a diffraction pattern being 5 min, a temperature range of about 2.5 K was covered in each acquisition.

Isothermal pressure scans. The pressure was varied in steps smaller than 30 MPa close to the ferroelectric transition and larger than 30 MPa out of the transition region. After each pressure step two successive acquisitions of 10 min were performed but only the second measurement was taken into account in order to let the system reach quasi-equilibrium conditions. The average rate of pressure change, 1.5 MPa min^{-1}, was chosen to produce the ferroelectric transition at a rate comparable to the temperature scan, i.e. 0.5 K min^{-1} (see below; the change in the Curie temperature induced by pressure was of the order of 0.35 K MPa^{-1}).

Effects of the phase transitions on the diffractograms

Figure 1 shows three typical diffraction patterns recorded during a heating run at ambient pressure (without pressure cell) in the ferroelectric phase, in the paraelectric phase and in the molten state. These diffractograms, over a broad Q range, have been obtained by scanning the angle of the multidetector in steps of 3° and regrouping the data into a single file. For the determination of the pressure–temperature phase diagram, only the Q range between 1 Å^{-1} and 1.6 Å^{-1} was analysed (with the multidetector in a fixed position) for three complementary reasons: (i) the most obvious

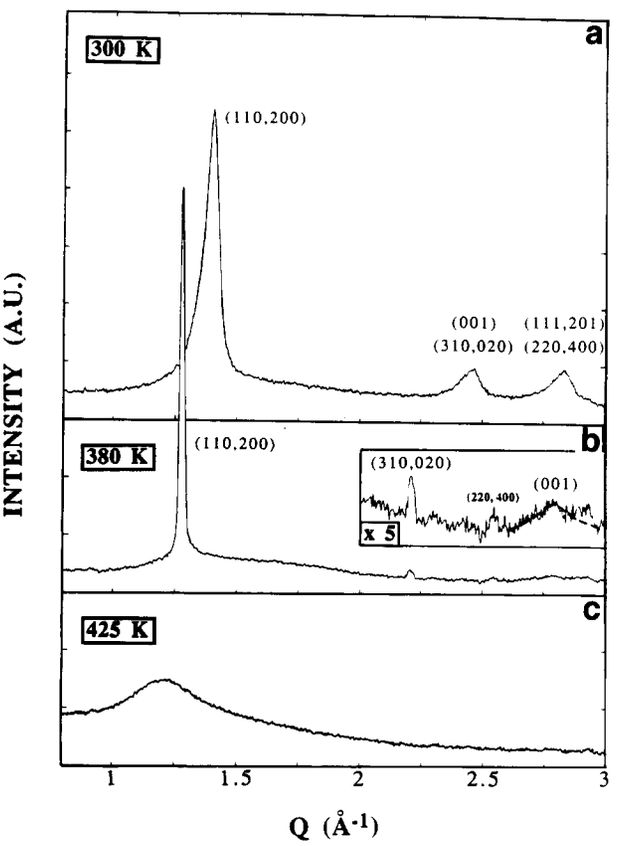

Figure 1 Neutron powder diffractograms of the 70/30 copolymer (during a heating run at ambient pressure): (a) in the ferroelectric phase (300 K); (b) in the paraelectric phase (380 K); (c) in the molten phase (425 K). The three plots are shown with the same scales

changes through the two phase transitions are observed around $Q=1.3$ Å^{-1}; (ii) the scanning procedure takes a much longer time; and (iii) spurious diffraction from the high pressure cell was also observed for $Q>2.5$ Å^{-1}.

A detailed analysis of the complete diffractograms of the three copolymers at ambient pressure has been reported elsewhere[15].

Data analysis

For refining the positions and the intensities of the Bragg peaks, especially in the transition region, where both the ferroelectric and the paraelectric phases coexist, we used a program named 'CURFIT'[16]. This program is based on a least-squares fit by linearization of the fitting function. Empirically we found that, in the Q range 1.0–1.6 Å^{-1}, the shapes of the ferroelectric and paraelectric Bragg peaks were better described by a Lorentzian function than by a Gaussian. Indeed, as is usual in semi-crystalline polymers, broad Bragg peaks were observed due to the very small size of the coherent crystalline regions, and hence the shapes of the Bragg peaks are mainly determined by the size distribution of the crystallites.

In the hexagonal paraelectric phase the rather narrow Bragg peak was fitted with a single Lorentzian characterized by its position Q_1, its integrated intensity I_1 and its full width at half maximum ΔQ_1 (*Figure 2a*).

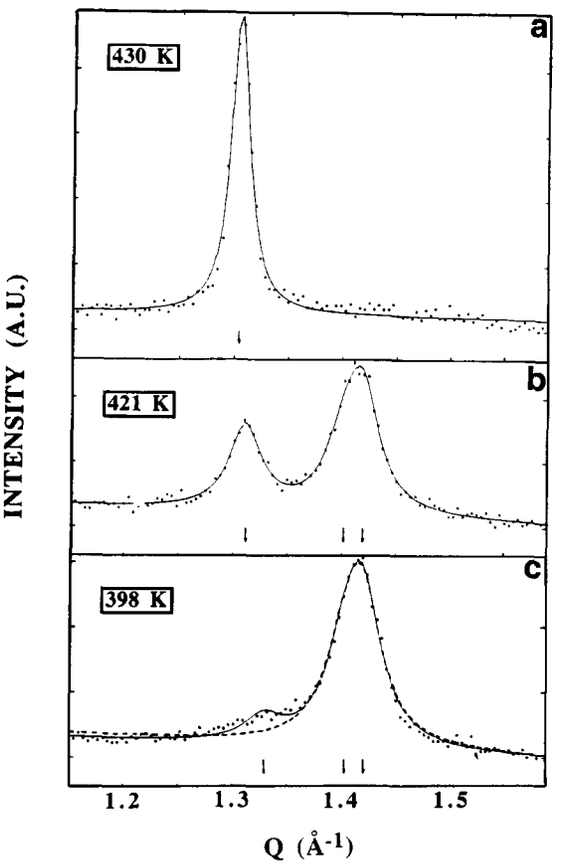

Figure 2 Neutron powder diffractograms (during a cooling run at 300 MPa) and fitted curves of the 70/30 copolymer: (a) in the paraelectric phase (430 K), single Lorentzian $Q_1=1.305$ Å^{-1}, $\Delta Q_1=0.020$ Å^{-1}; (b) in the coexistence region (421 K), single Lorentzian $Q_1=1.311$ Å^{-1}, $\Delta Q_1=0.035$ Å^{-1} and double Lorentzian $Q_{110}=1.419$ Å^{-1}, $\Delta Q_{110}=0.037$ Å^{-1}, $q=0.018$ Å^{-1}, $k=0.5$; (c) in the ferroelectric phase (398 K), double Lorentzian $Q_{110}=1.420$ Å^{-1}, $\Delta Q_{110}=0.041$ Å^{-1}, $q=0.018$ Å^{-1}, $k=0.5$

No special constraint in the least-squares procedure was imposed.

In the pseudo-hexagonal ferroelectric phase (*Figure 2c*) the asymmetry of the Bragg peak is mainly due to the splitting of the reflections (110) and (200)[15]. Hence a double Lorentzian peak ($L_{110}+L_{200}$) was used for profile fitting with parameters constrained in the following way

$$I_{200}=kI_{110}$$
$$Q_{200}=Q_{110}-q$$
$$\Delta Q_{110}=\Delta Q_{200}$$

where the parameters k and q were fixed according to the structural data presented in ref. 15 (e.g. $k=0.5$ and $q=0.018$ Å^{-1} for the copolymer of composition 70/30).

This procedure was chosen in order to limit the number of fitted parameters, especially in the temperature range of phase coexistence (*Figure 2b*), where the diffraction patterns were fitted with a paraelectric and a ferroelectric peak chosen as described above. When only the ferroelectric phase is present in the sample it is clear from *Figure 2c* that the double Lorentzian $L_{110}+L_{200}$ (broken line) does not adequately describe the additional scattering around 1.33 Å^{-1} attributed to the amorphous phase. Alternatively, a fit including a paraelectric peak (full line) converges towards a non-zero intensity at the same position. Owing to this ambiguity, the results of this last fitting procedure were discarded when the intensity of the paralectric peak was smaller than 20% of its maximum value.

The diffraction pattern of the molten phase (*Figure 1c*) does not provide an appropriate template for describing the scattering function of the amorphous phase at any temperature since it appears that the line shape and the position of the amorphous halo change when the crystalline regions undergo a phase transition[3]. Moreover, owing to the large width of the halo ($\Delta Q>0.3$ Å^{-1}), it cannot be adequately fitted in the restricted Q range investigated. A reliable description of the amorphous halo is thus difficult to establish from the data presented here. Therefore, to simplify the fitting procedure in the restricted Q range of interest, both the incoherent scattering and the coherent scattering from the amorphous phase were accommodated using a straight background whose level and slope were fitted parameters.

Figure 2 displays examples of experimental data together with the fitted curves. Even if the agreement is not fully satisfactory for individual sets of data, it must be emphasized that the aim of this treatment was to analyse series of diffractograms (approximately 600 for each composition) in order to observe *changes* induced by pressure and temperature. Therefore, although the simplified fitting procedure chosen may introduce systematic errors in absolute position, intensity or width of the Bragg peaks, we consider that it is accurate in revealing *relative* changes in these quantities.

PRESENTATION AND ANALYSIS OF THE RESULTS

We first detail the results obtained with the copolymer of composition 70/30 mol% and then describe the differences observed with the other two compositions, namely 80/20 and 60/40 mol%.

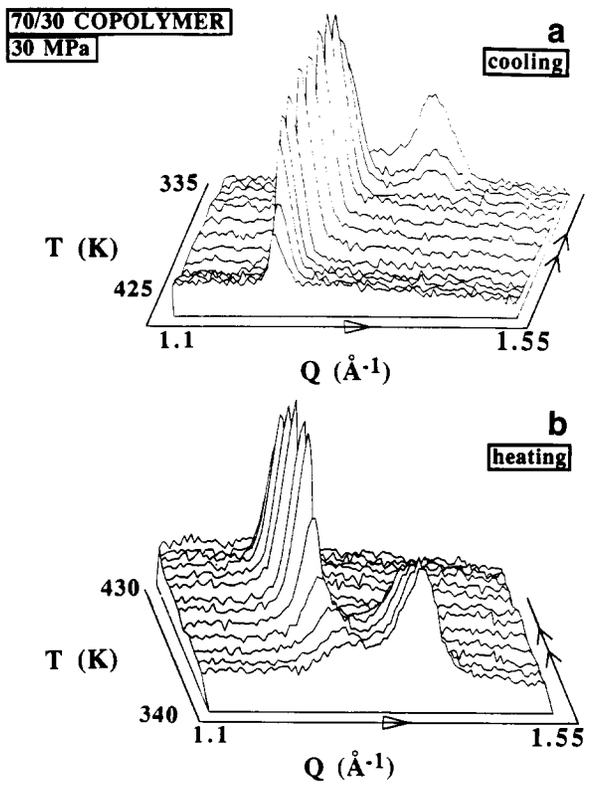

Figure 3 Series of neutron powder diffractograms of the 70/30 copolymer at 30 MPa in the Q range 1.1–1.55 $Å^{-1}$: (a) cooling run from 425 K to 335 K; (b) heating run from 340 K to 430 K

70/30 copolymer

Figure 3 shows the evolution of the powder diffraction pattern, at 30 MPa, during a heating and cooling run.

The first diffraction pattern of *Figure 3* (bottom) reveals at about $Q = 1.4\ Å^{-1}$ the composite Bragg reflection (200 + 110) of the ferroelectric phase and, near $Q = 1.3\ Å^{-1}$, a low intensity peak corresponding to the appearance of the paraelectric phase. As the temperature is raised a transformation from ferroelectric to paraelectric phase gradually takes place and is completed at 395 K. Upon further heating, the intensity of the paraelectric peak remains almost constant over 20 K and finally decreases abruptly owing to the melting.

It is worth noting that, for this composition, the ferroelectric transition and the melting are clearly separated, the ferroelectric peak vanishing completely before the paraelectric peak starts to decrease.

If we now examine the cooling run from the molten state (*Figure 3*, top), we observe that the polymer crystallizes rapidly and that the paraelectric phase remains stable over a much wider range of temperatures (about 50 K), the ferroelectric transition taking place below 355 K.

A more quantitative description of this behaviour is obtained from the results of the least-squares fits. Owing to the difference in the integrated intensities between the ferroelectric and the paraelectric Bragg reflections, the temperature dependence of the total integrated intensity (*Figure 4a*) clearly shows the two phase transitions and the hysteresis phenomena observed upon heating and cooling at constant pressure. Similarly, the pressure dependence of the total intensity at constant temperature shows the hysteresis of the ferroelectric transition: at 410 K the copolymer is in the paraelectric phase at low pressure and in the ferroelectric phase at high pressure (*Figure 4b*). The total intensity is the same after temperature or pressure cycling and this demonstrates the reversibility of the phase transition and of the degree of crystallinity (after preliminary cycling[3]).

The difference between the integrated intensities of the ferroelectric and the paraelectric phases can be partly attributed to different degrees of crystallinity in the two phases (the degree of crystallinity has been reported to be about 10% lower in the paraelectric phase[3]). But the main reason for this difference is a change in the neutron structure factor of the composite (200 + 110) Bragg reflection. This is justified by the fact that a much smaller difference is observed in the X-ray structure factors[3].

In order to analyse these data in terms of volume fractions of the two phases we must first consider that out of the transition region, i.e. either in the homogeneous ferroelectric or paraelectric phase, the integrated intensity decreases almost linearly with increasing temperature or with decreasing pressure. This is attributed to the Debye–Waller factor $D = \exp[-B(Q/4\pi)^2]$, which accounts for the reduction of the structure factor owing to thermal motions of the atoms about their equilibrium positions. For a given Bragg reflection the temperature factor B is proportional to the mean-square displacement of the atoms perpendicular to the Bragg planes, i.e. $B = 8\pi^2\langle u_\perp^2 \rangle$, which increases with temperature and decreases with pressure. From the observed changes in the integrated

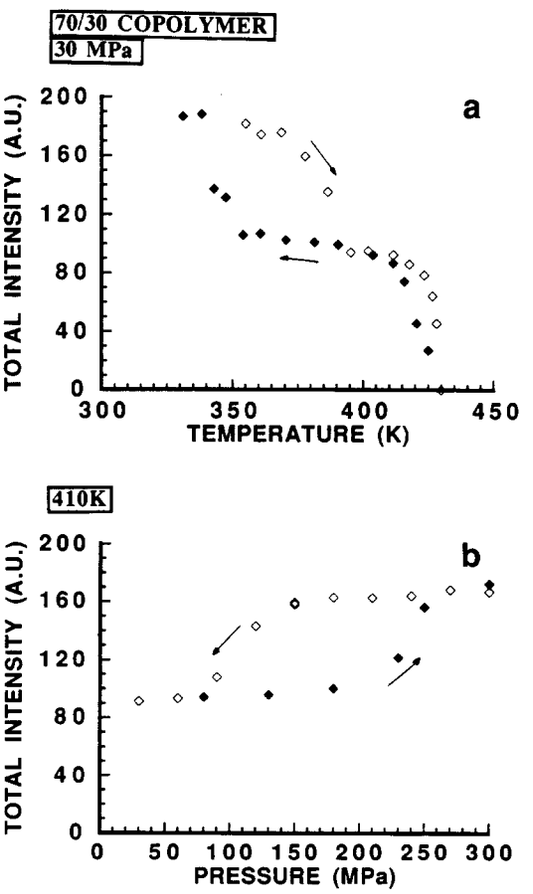

Figure 4 Total integrated intensity of the (200 + 110) Bragg peaks (ferroelectric and paraelectric) of the 70/30 copolymer: (a) *versus* temperature at 30 MPa for (◇) heating and (◆) cooling runs; (b) *versus* pressure at 410 K for (◇) decreasing and (◆) increasing pressure

intensity one can get

$$\frac{\partial B}{\partial T}=\frac{8\pi^2}{Q^2}\left(\frac{1}{I}\frac{\partial I}{\partial T}\right)$$

and

$$\frac{\partial B}{\partial P}=\frac{8\pi^2}{Q^2}\left(\frac{1}{I}\frac{\partial I}{\partial P}\right)$$

According to our whole set of measurements under isobaric or isothermal conditions we obtain

$\partial B/\partial T=0.13\ \text{Å}^2\ \text{K}^{-1}$ and $\partial B/\partial P=-0.024\ \text{Å}^2\ \text{MPa}^{-1}$

in the paraelectric phase and

$$\partial B/\partial T=0.05\ \text{Å}^2\ \text{K}^{-1} \text{ and } \partial B/\partial P\approx 0$$

in the ferroelectric phase.

Concerning the ferroelectric phase, one may remark that a linear extrapolation to 0 K gives $B=15\ \text{Å}^2$ at room temperature, a value in good agreement with that obtained from powder diffraction results at room temperature[15]. The results obtained in the paraelectric phase are consistent with a higher disorder vanishing through a phase transition (well above 0 K), and the effect of pressure on the Debye–Waller factor is attributed to a higher compressibility of the lattice (see *Table 1*).

A more detailed insight into the phase transition mechanism is obtained in considering the evolution of the volume fraction of each phase as deduced from the integrated intensity of each Bragg reflection (divided by the Debye–Waller factor). The results plotted in *Figure 5a* show the transformations upon heating and cooling and the broad ranges of phase coexistence (of about 25 K and 15 K, respectively), as well as the extended temperature range of melting (and crystallization) characteristic of polymeric materials. Between the cooling and the heating runs a large hysteresis of about 40–50 K is observed for the ferroelectric transition while a smaller hysteresis, of about 10 K, is observed between melting and recrystallization. *Figure 5b* shows a similar behaviour for the ferroelectric transition under pressure: for decreasing pressure the transition extends over 60 MPa and for increasing pressure it extends only over 40 MPa, the hysteresis being about 120 MPa. Let us remark, however, that in this pressure scan the transition is not complete.

For such diffuse transitions there is no clear agreement in the literature of the definition of a mean transition temperature, except perhaps for the case of binary mixtures for which the starting point, the end point, and the rate of transformation are thermodynamically well defined. In our case we have a spread of transition temperatures which comes from the inhomogeneous character of the material (distribution of size of the crystallites, inhomogeneities in comonomer compositions and strain fields[17]). Such a system never reaches real thermodynamic equilibrium in a finite time and one can only reduce the kinetic effects by using slow transformation rates. Even so, the volume fractions evolve smoothly without clear-cut starting points and end points. The mean transition temperature could then be defined by the maximum transformation rate corresponding to the inflection points of the volume fractions and to the maximum of the specific heat anomaly; alternatively, it is also possible to define it as the midpoint of the transformation, i.e. as the temperature for which the volume fraction of the transformed phase is 50%.

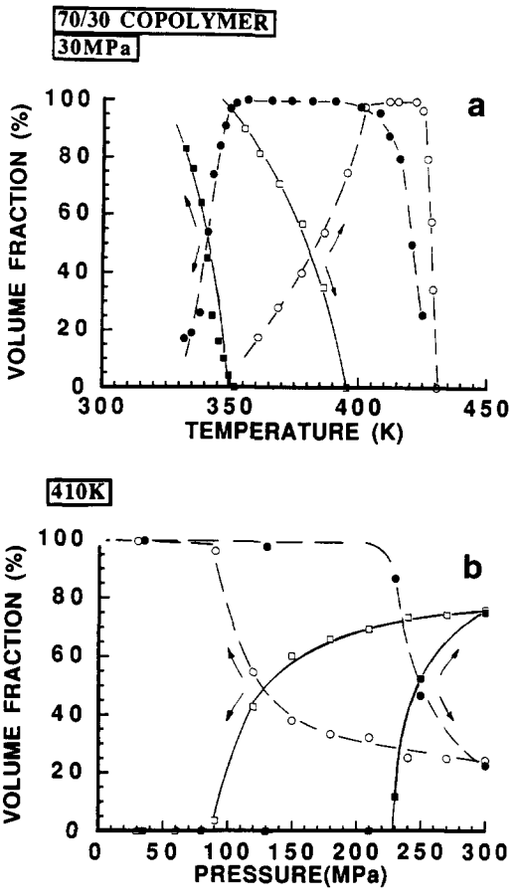

Figure 5 Relative contents of the ferroelectric (F) and paraelectric (P) phases in the 70/30 copolymer: (a) *versus* temperature at 30 MPa (□ F, ○ P) upon heating and ■ F, ● P) upon cooling; (b) *versus* pressure at 410 K (□ F, ○ P) for decreasing pressure and (■ F, ● P) for increasing pressure

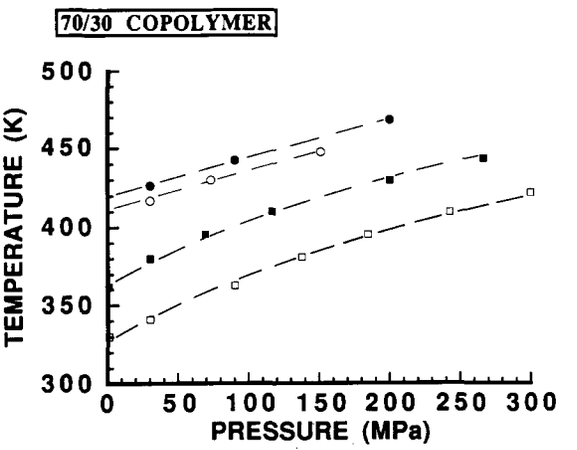

Figure 6 Phase diagram of the 70/30 copolymer showing the ferroelectric and melting transitions: Curie temperatures upon heating (■) and upon cooling (□); melting temperatures (●) and crystallization temperatures (○)

From our experimental data, this last definition is more precise and we have used it to draw the pressure–temperature phase diagram shown in *Figure 6*.

Upon increasing pressure the same phase transition behaviour is observed but at a correspondingly higher temperature. Therefore, the Curie temperature increases (both upon heating and cooling), suggesting greater stability of the low temperature phase. This is what is expected from the specific volume increase through the

ferroelectric transition[3,17]. Similarly, the melting and the crystallization temperatures increase under pressure in consistency with the fact that pressure favours the more compact structure.

The phase diagram of *Figure 6* also shows that the thermal hysteresis of the ferroelectric transition as well as that of melting–crystallization remains almost unchanged in the observed pressure range, although the ferroelectric transition lines are not straight. From the slopes at low pressure (< 100 MPa) we obtain

$$dT_{C+}/dP \approx dT_{C-}/dP = 0.38 \text{ K MPa}^{-1}$$

$$dT_M/dP \approx dT_\chi/dP = 0.25 \text{ K MPa}^{-1}$$

indicating a clear decrease in the range of stability of the paraelectric phase with increasing pressure. At higher pressures the slope of the ferroelectric transition lines decreases down to about 0.28 K MPa^{-1} and thus a merging of the two transition lines could be expected only at a much higher pressure.

Concerning the pressure dependence of the Curie temperature, the above values are close to those reported by Samara[11] from dielectric measurements on a 70/30 mol% copolymer ($dT_C/dP = 0.30 \pm 0.02$ K MPa^{-1} upon heating and cooling) and those reported by Akashige *et al.*[12] from X-ray diffraction on a 73/27 mol% copolymer ($dT_C/dP \approx 0.35$ K MPa^{-1}). But concerning the melting temperature, Samara[11] found a transition line corresponding to $dT_M/dP \approx 0.5$ K MPa^{-1} (at low pressure), a result which led him to conclude that the range of stability of the paraelectric phase increases under pressure. Our results based on the vanishing of the diffraction peaks through the melting point clearly disagree with his conclusions.

The ferroelectric transition is accompanied by a large change of the unit cell parameters and this can be observed in the temperature dependence of the d spacing of the composite (200 + 110) Bragg reflection in the ferroelectric and paraelectric phases. *Figure 7* displays the results at 30 MPa: upon heating the d spacing perpendicular to the chain axis increases by 9% (in the middle of the coexistence region), while d_{001} (along the chain axis direction) decreases by 10%[5]. This results in a volume change

$$(V_{para} - V_{ferro})/V_{ferro} = +6.7\% \qquad T_{C+} = 380 \text{ K}$$

It is worth pointing out that upon cooling a smaller volume change is observed (owing to the different thermal expansion coefficients of the two phases)

$$(V_{ferro} - V_{para})/V_{ferro} = -4.9\% \qquad T_{C-} = 342 \text{ K}$$

Figure 7 also demonstrates that in the ferroelectric phase ordinary thermal expansion is observed and that the results obtained upon heating and cooling fall almost onto the same straight line over the whole range of temperatures. On the contrary, in the paraelectric phase, the behaviour of the lattice spacing appears to be different upon cooling and upon heating. Combined with the evolution of the volume fractions (*Figure 5a*), one can see that linear thermal expansion is observed (with a rather large slope) when the volume fraction of the paraelectric phase Φ_{para} is higher than 80%, while at the first stages of its growth the paraelectric lattice is compressed. Indeed, the growth of this phase of higher specific volume is somehow self-hindered inside the ferroelectric matrix and this perhaps provides an explanation of why the range of phase coexistence is broader upon heating (40 K) than upon cooling (20 K)[3,17].

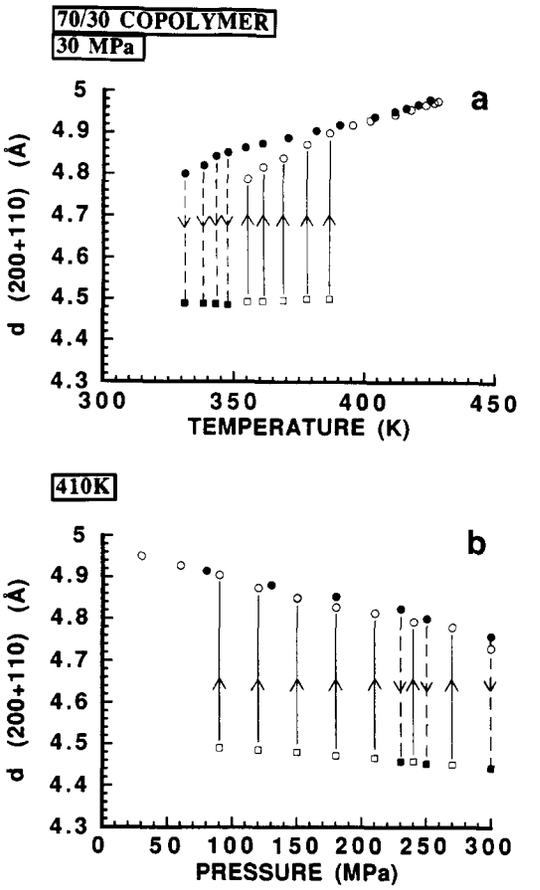

Figure 7 Ferroelectric (F) and paraelectric (P) (200 + 110) d spacings through the ferroelectric transition of the 70/30 copolymer (the lines show the coexistence of the two phases and the arrows show the evolution): (a) *versus* temperature at 30 MPa (□ F, ○ P) upon heating and (■ F, ● P) upon cooling; (b) *versus* pressure at 410 K (□ F, ○ P) for decreasing pressure and (■ F, ● P) for increasing pressure

The change in the d spacings under hydrostatic pressure (*Figure 7b*) also allows an analysis of the lattice compressibility, which appears to be about 2.5 times higher in the paraelectric phase than in the ferroelectric phase.

80/20 copolymer

In the copolymer with 20% TrFE the Curie temperature is very close to the melting point. Isobaric temperature scans (at eight different pressures) through both the ferroelectric transition and the melting–crystallization were then performed. At high pressure, upon cooling from the melt, the copolymer crystallizes in the paraelectric phase (*Figure 8*) and further transforms into the ferroelectric phase. But, upon heating, the melting occurs prior to complete transformation from the ferroelectric to the paraelectric phase.

For the profile fitting of these data it was found empirically that a single Lorentzian peak was sufficient to describe the composite ferroelectric Bragg peak (200 + 110). The results of these fits provide first the integrated intensities from which the volume fractions of the ferroelectric and paraelectric phases are calculated (after evaluation of the Debye–Waller factor). *Figure 9* displays the results obtained for low and high pressure.

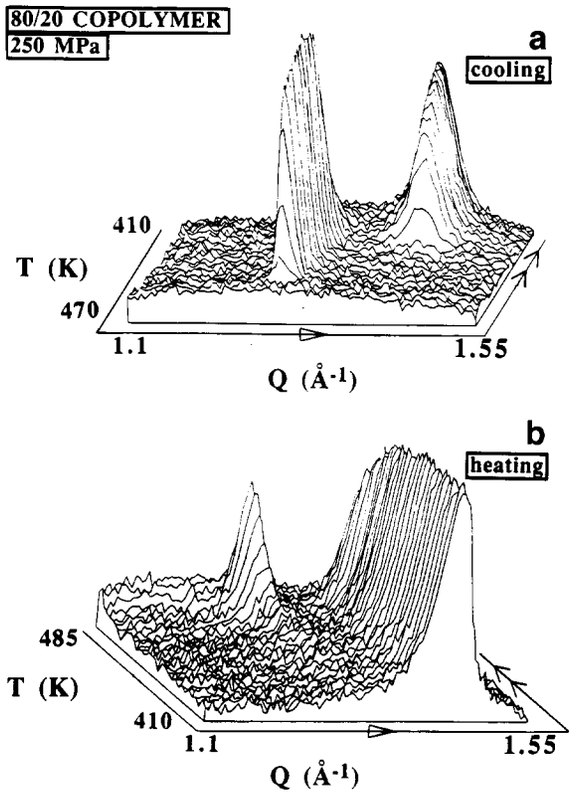

Figure 8 Series of neutron powder diffractograms of the 80/20 copolymer at 250 MPa in the Q range 1.1–1.55 $Å^{-1}$: (a) cooling run from 470 K to 410 K; (b) heating run from 410 K to 485 K

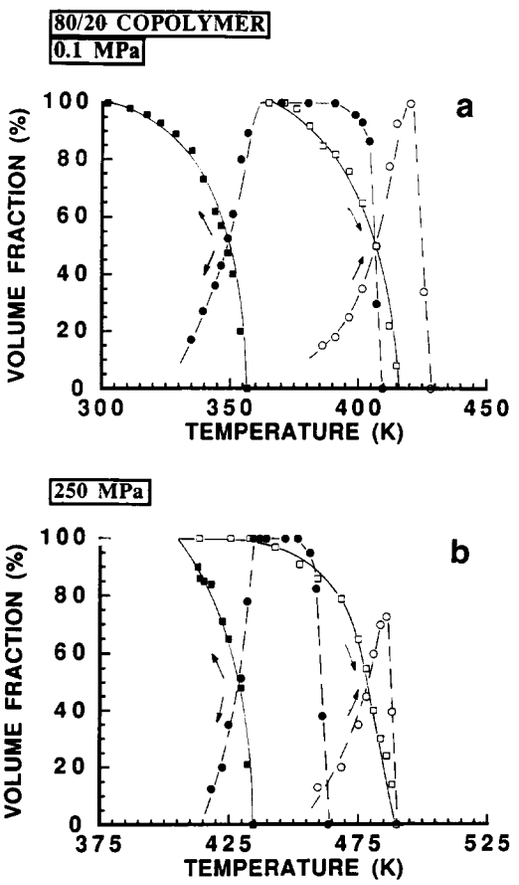

Figure 9 Relative contents of ferroelectric (F) and paraelectric (P) phases in the 80/20 copolymer *versus* temperature (□ F, ○ P) upon heating and (■ F, ● P) upon cooling: (a) at 0.1 MPa; (b) at 250 MPa

Upon heating at atmospheric pressure the ferroelectric transition starts at around 370 K and is just complete at 415 K when melting of the paraelectric phase occurs. Thus the midpoints of these two successive transformations are only 19 K apart. Upon cooling at a rate of about 0.5 K min^{-1} the crystallization of the paraelectric phase is observed 18 K below its melting point, and this undercooling is noticeably higher than in the 70/30 copolymer. Additionally, the ferroelectric transition shows a large thermal hysteresis of almost 60 K.

At high pressure (250 MPa) the transition points are shifted to higher temperatures and the Curie temperature gets closer to the melting point in such a way that the ferroelectric transition is no more complete upon heating. This means that some ferroelectric crystallites melt without transforming into the paraelectric phase. Indeed, in the pressure–temperature phase diagram a triple point is expected above which a single line would correspond to the melting of the ferroelectric phase. The distribution of transition temperatures from one crystallite to another results therefore in a distribution of triple points. The results in *Figure 8* show that about 30% of the crystallites have their triple points at a pressure lower than 250 MPa. Moreoever, upon cooling from the melt, the temperature range of the paraelectric phase shrinks under pressure. It is then expected, from an extrapolation, that above 500–600 MPa the 80/20 copolymer would no longer crystallize into the paraelectric phase but, very probably, into the α phase, as for copolymers of lower TrFE contents at atmospheric pressure[18].

From the results obtained at different pressures a phase diagram can be drawn using the same convention as defined above for the midpoints of the transitions. Thus, the transition lines represented in *Figure 10* describe the behaviour of a 'middle crystallite' which transforms when just 50% of the total volume has been transformed. In such a representation the ferroelectric transition line and the melting transition line should cross at a triple point when the maximum volume fraction of the paraelectric phase becomes less than 50%. From an extrapolation of the data obtained between 0.1 and 250 MPa this triple point is estimated to be at $P^* \approx 500$ MPa and $T^* \approx 560$ K upon heating.

Figure 10 also shows that, as for the 70/30 copolymer,

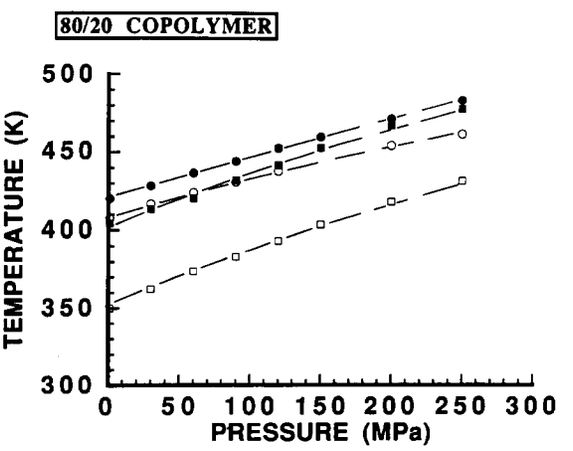

Figure 10 Phase diagram of the 80/20 copolymer showing the ferroelectric and melting transitions: Curie temperatures upon heating (■) and upon cooling (□); melting temperatures (●) and crystallization temperatures (○)

the transition lines are not straight. Indeed, for the slopes at low pressure (< 100 MPa) one gets

$$dT_{C+}/dP = 0.32\ \text{K MPa}^{-1}$$

and

$$dT_M/dP = 0.27\ \text{K MPa}^{-1}$$

whose linear extrapolation would place the triple point upon heating at $P^* \approx 350$ MPa.

In addition, for both transitions the thermal hysteresis appears to change with pressure: for the ferroelectric transition upon cooling one gets a higher slope at low pressure

$$dT_{C-}/dP = 0.36\ \text{K MPa}^{-1}$$

but the two lines become almost parallel at high pressure, as for the 70/30 copolymer. The thermal hysteresis of the ferroelectric transition does not depend much on pressure

$$T_{C+} - T_{C-} \approx 50\ \text{K}$$

Moreover, the difference between the melting and crystallization temperatures surprisingly increases with pressure, and this could be related to the fact that at high pressure the melting of the paraelectric phase coexists with the melting of the ferroelectric phase.

For this copolymer a larger volume change occurs during the ferroelectric transition as can be seen in *Figure 11*, where the *d* spacing of the composite (200 + 110) Bragg reflection is presented (at 0.1 MPa and at 250 MPa). At atmospheric pressure the contraction (expansion) of the *a* and *b* lattice parameters through the transition reaches −8.8% upon cooling (and +11.3% upon heating). Thus the volume of the unit cell contracts by 7.6% upon cooling and expands by 10% upon heating. As already mentioned for the 70/30 copolymer, such a large volume increase produces internal strains in the coexistence region. It is visible in *Figure 11* that, upon heating, the lattice spacing of the first nuclei of the paraelectric phase is compressed by about 0.8% with respect to its equilibrium value (measured at the same temperature upon cooling). This compressive strain, which can be described by an internal pressure as high as 120 MPa, decreases as the paraelectric phase grows. At (external) atmospheric pressure, it almost vanishes when the paraelectric volume fraction is larger than 80%. However, under high (external) pressure the maximum volume fraction of the paraelectric phase remains below 70%. The further volume increase owing to melting seems to maintain a noticeable internal pressure in the range of coexistence of the two solid phases with the molten phase. This effect explains the upwards shift of the melting temperature with respect to the crystallization temperature and also the apparent triggering of the melting of the paraelectric phase by the melting of the ferroelectric phase (*Figure 9*).

60/40 copolymer

Owing to the complex phase transition behaviour of the 60/40 mol% copolymer at low pressure, we shall first discuss the results obtained at high pressure.

At 300 MPa, the evolution of the composite Bragg reflection (200 + 110) through the ferroelectric transition (*Figure 12*) is similar to that observed for the 70/30 mol% and the 80/20 mol% copolymers at low pressure. It is, however, worth noting that, in the phase transition region,

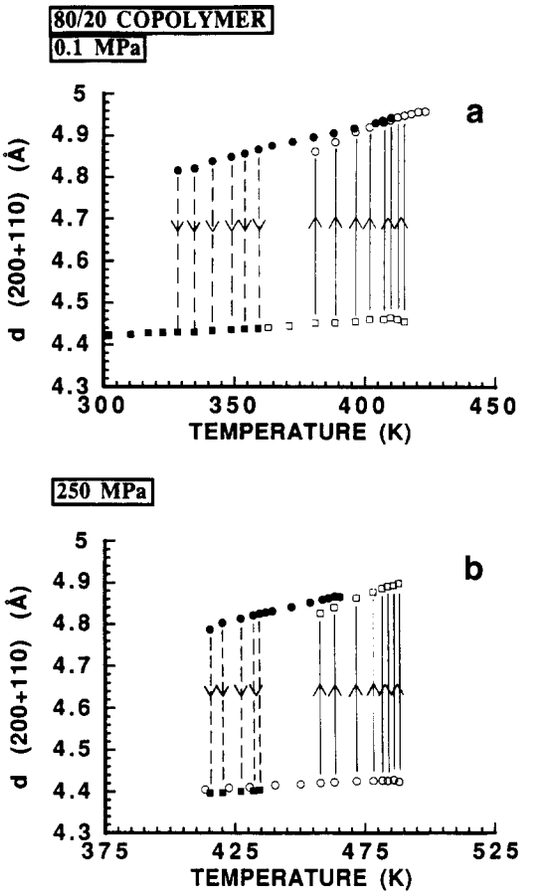

Figure 11 Ferroelectric (F) and paraelectric (P) (200 + 110) *d* spacings through the ferroelectric transition of the 80/20 copolymer *versus* temperature (□ F, ○ P) upon heating and (■ F, ● P) upon cooling (the lines show the coexistence of the two phases and the arrows show the evolution): (a) at 0.1 MPa; (b) at 250 MPa

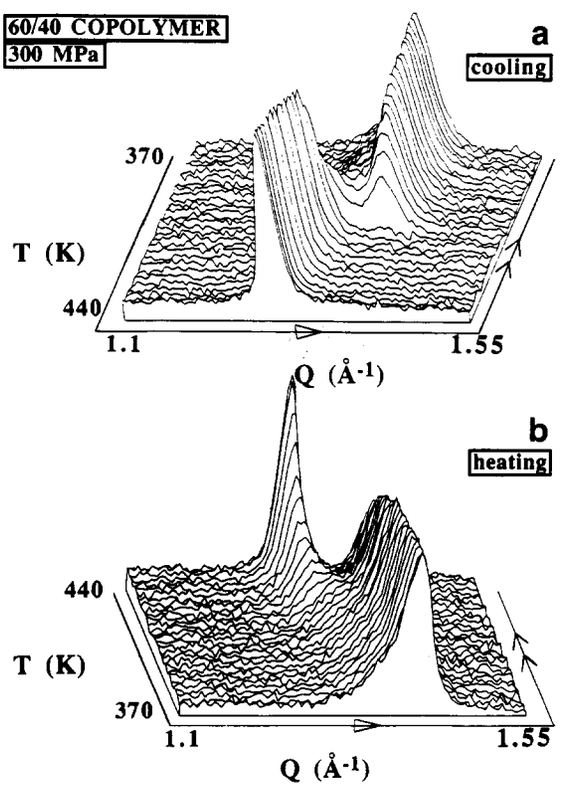

Figure 12 Series of neutron powder diffractograms of the 60/40 copolymer at 300 MPa in the *Q* range 1.1–1.55 Å^{-1}: (a) cooling run from 440 K to 370 K; (b) heating run from 370 K to 440 K

the Q separation between the low and the high temperature Bragg peaks is less clear. This could be partly attributable to a smaller variation of the lattice parameters between the ferroelectric and the paraelectric phases[15], but it is also apparent from *Figure 12* that, upon heating, the high temperature peak seems to arise as a shoulder on the ferroelectric peak. This effect is even more pronounced at low pressure (*Figure 13*), where the high temperature peak seems to persist down to room temperature.

In order to describe this effect we have considered for the fitting procedure a double Lorentzian ($L_{110}+L_{200}$) corresponding to the ferroelectric peak and another Lorentzian, which we shall call the 'disordered' peak, corresponding to the evolution of the high temperature peak.

The results obtained for the volume fractions at 300 MPa (*Figure 14a*) are comparable to those obtained with the two other copolymers, but the evolution of the lattice parameter (*Figure 14b*) shows an anomalous behaviour for the 'disordered phase'. When this phase appears (around 380 K) the interchain distance of 4.65 Å is small, but between 415 K and 430 K an increase of about 1.7% is observed towards the expected d spacing of the paraelectric phase. Upon cooling the same behaviour is observed with a thermal hysteresis of 15 K, noticeably smaller than that exhibited by the volume fractions (25 K).

These results suggest the existence of a phase transition between the paraelectric phase and another 'low temperature disordered' (LTD) phase. Thus the d spacing given by the fitting procedure corresponds to an average between the paraelectric and the LTD phases. Alternatively, the diffraction data have also been analysed

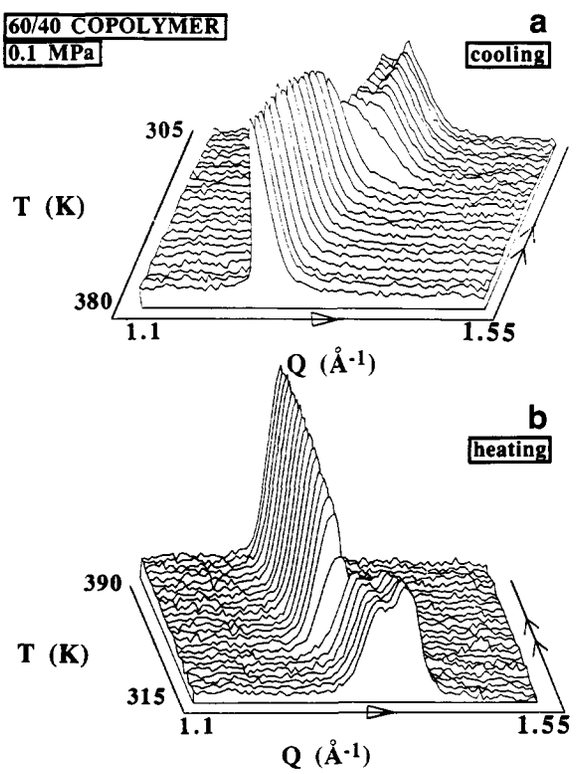

Figure 13 Series of neutron powder diffractograms of the 60/40 copolymer at 0.1 MPa in the Q range 1.1–1.55 $Å^{-1}$: (a) cooling run from 380 K to 305 K; (b) heating run from 315 K to 390 K

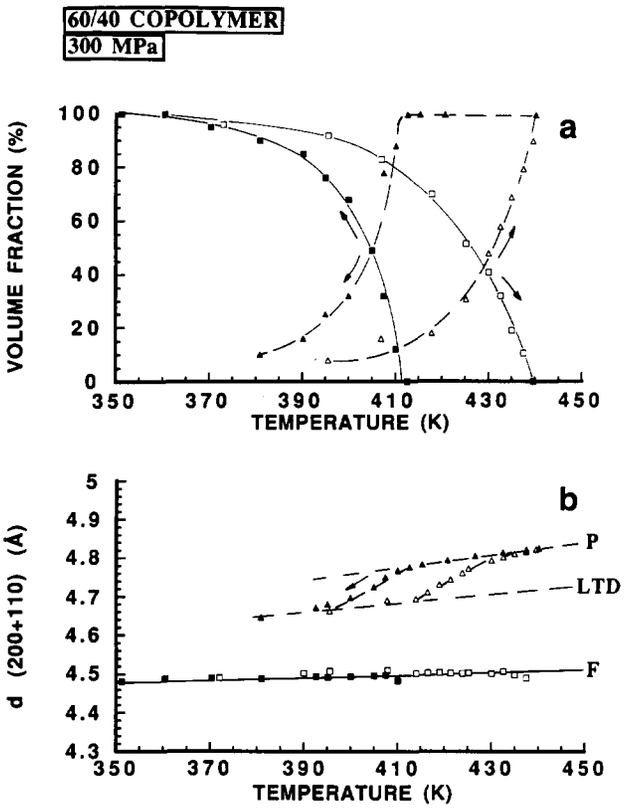

Figure 14 Temperature dependence of the ferroelectric (F) and the 'disordered' (D) phases of the 60/40 copolymer at 300 MPa (□ F, △ D) upon heating and (■ F, ▲ D) upon cooling: (a) relative contents of each phase; (b) (200 + 110) d spacings

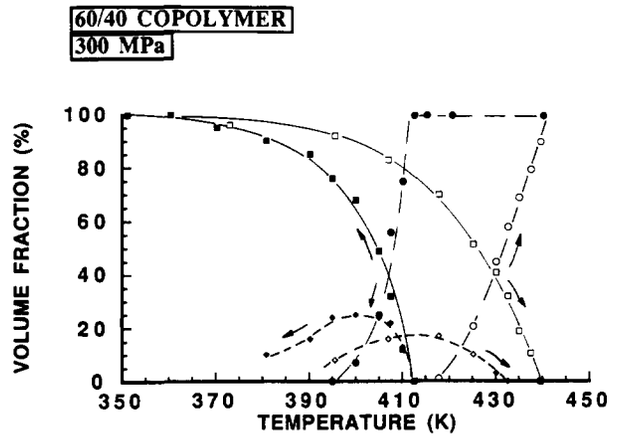

Figure 15 Relative contents of the ferroelectric (F), low temperature disordered (LTD) and paraelectric (P) phases of the 60/40 copolymer at 300 MPa *versus* temperature: (□ F, ◇ LTD, ○ P) upon heating; (■ F, ◆ LTD, ● P) upon cooling

considering three phases (F, LTD and P) whose d spacings obey linear thermal expansions, as represented by the straight lines in *Figure 14b*.

According to this description, the evolution of the three volume fractions is shown in *Figure 15*. Upon heating, up to 417 K, the decrease in the ferroelectric fraction corresponds to the emergence of the LTD phase. Above 417 K, both the LTD and the ferroelectric phases transform into the paraelectric phase. Upon cooling, the transformation of the paraelectric phase gives rise to the simultaneous appearance of the LTD and ferroelectric phases, but at lower temperatures only the ferroelectric phase remains. Therefore, both upon heating and cooling, three different phase transitions occur.

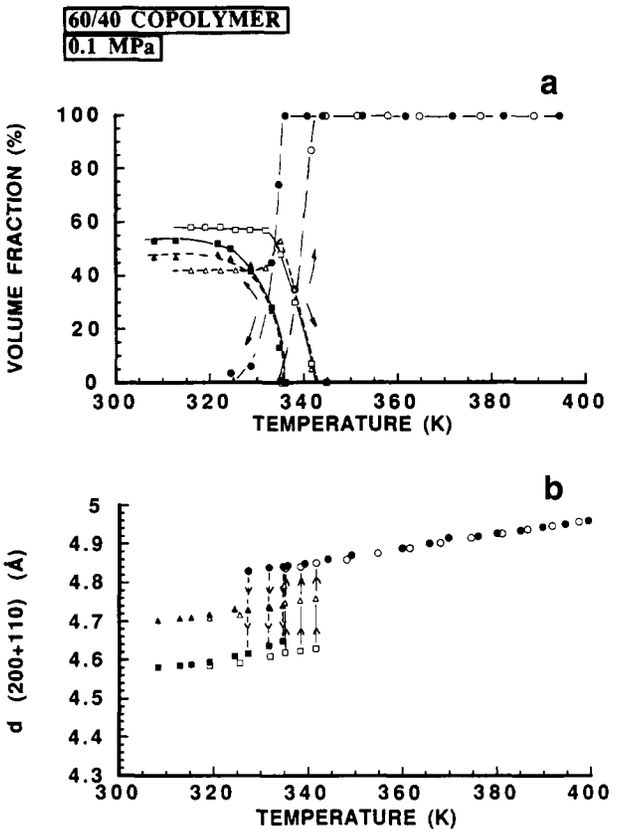

Figure 16 Temperature dependence of the ferroelectric (F), low temperature disordered (LTD) and paraelectric (P) phases of the 60/40 copolymer at 0.1 MPa (□ F, △ LTD, ○ P) upon heating and (■ F, ▲ LTD, ● P) upon cooling: (a) relative contents of each phase; (b) (200+110) *d* spacings

Following the same procedure, we can now discuss the results at atmospheric pressure. *Figure 16* shows the evolution of the volume fractions and the lattice parameters of each phase. As is also visible in *Figure 13*, the LTD phase persists down to room temperature and its volume fraction seems to reach an equilibrium value (around 40–50%). This value, which clearly decreases with increasing pressure, actually depends on the thermal history of the sample, showing the metastable nature of the LTD phase.

The evolution of the volume fractions is very similar upon heating and cooling with a hysteresis of only 7 K. In addition, the transformation of the paraelectric phase is very abrupt (over less than 10 K) and the growth of the ferroelectric and LTD phases is nearly simultaneous. It is also worth noting that, upon heating, the ferroelectric phase partly transforms into the LTD phase, as already seen at high pressure.

The analysis of the ferroelectric *d* spacing under pressure (*Figure 17*) shows that, whereas at high pressure the evolution is consistent with the observed compressibility of the 70/30 mol% copolymer, at low pressure there is an additional expansion. This expansion is attributed to the coexistence of the ferroelectric and LTD phases and disappears after electrical poling, when only the ferroelectric phase is present[15]. This is analogous to the behaviour observed when a large number of defects are present in the crystalline regions[19]. Moreover, the small coherence length of the ferroelectric phase along the chain axis[15] suggests a lamellar substructure of alternating LTD and ferroelectric regions along the chain axis direction. This could explain the simultaneous appearance of the two phases upon cooling from the paraelectric phase.

Our results demonstrate that, with decreasing pressure, the room temperature structure evolves from a pure ferroelectric phase towards a close mixture of a 'distorted' ferroelectric phase with a new phase (LTD), the fraction of which may change with temperature and pressure. From X-ray diffraction measurements on oriented specimens with low VDF contents, Tashiro *et al.*[5] have considered a single, low temperature phase including a kind of micro-twinning along the chain axis – the so-called 'cooled phase'. Our results show that, even with a comparable arrangement, the coexistence of two phases of different symmetries has to be taken into account.

In addition, the evolution of the volume fractions upon heating shows that some of the ferroelectric regions undergo a Curie transition while the rest of them transform first into the LTD phase and then into the paraelectric phase. Therefore a triple point is expected in the pressure–temperature phase diagram, corresponding to the crossing of the ferroelectric–LTD and the LTD–paraelectric transition lines. From the results obtained at different pressures, the volume fraction of the LTD phase does not reach more than 50%. Thus, according to the criteria used for the midpoint of the transition, the triple point should not appear in the phase diagram. It is thus only possible to define one transition line, for which the volume fraction of the transformed phase is 50% (ferroelectric phase upon heating and paraelectric phase upon cooling) (*Figure 18*).

Probably owing to the metastable mixture of phases, the transition points are scattered and it is not possible to detect a curvature of the transition line. From the evolution of the transition temperature we obtain

$$dT_{C+}/dP = 0.31 \text{ K MPa}^{-1}$$

$$dT_{C-}/dP = 0.26 \text{ K MPa}^{-1}$$

and

$$dT_M/dP \approx dT_\chi/dP = 0.27 \text{ K MPa}^{-1}$$

indicating an increase in the thermal hysteresis upon increasing pressure, as observed by Akashige *et al.*[12] for the 54/46 mol% copolymer.

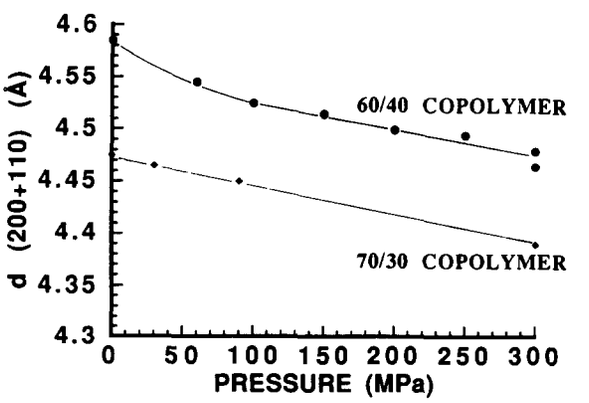

Figure 17 Pressure dependence of the ferroelectric (200+110) *d* spacing at room temperature: (●) 60/40 copolymer; (◆) 70/30 copolymer

DISCUSSION

In order to obtain a more detailed insight into the effect of the copolymer composition on the crystalline structure and on the ferroelectric–paraelectric phase transition, we have compared the measurements performed at a pressure of 200 MPa (for which the three copolymers exhibit a clear ferroelectric transition). *Figure 19* displays schematically the behaviour of the *d* spacing perpendicular to the chain axis direction for the three copolymers of composition 80/20, 70/30 and 60/40 mol%.

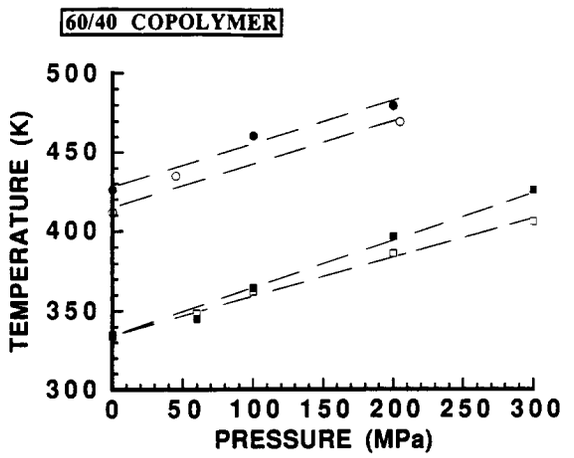

Figure 18 Phase diagram of the 60/40 copolymer showing the ferroelectric and melting transitions: Curie temperatures upon heating (■) and upon cooling (□); melting temperatures (●) and crystallization temperatures (○)

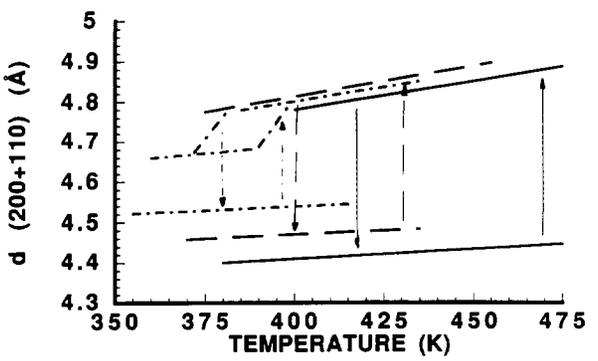

Figure 19 Schematic representation of the temperature dependence of the (200+110) *d* spacing through the ferroelectric transition at 200 MPa for the three copolymers: (——) 80/20; (– –) 70/30; (– · –) 60/40

From the temperature dependence of the *d* spacing, the linear thermal expansion coefficients $\alpha_{L,F}$ and $\alpha_{L,P}$ can be determined for the ferroelectric and paraelectric crystalline phases, respectively (*Table 1*). It appears that these coefficients are very similar for the three copolymers, with a thermal expansion about three times larger in the paraelectric phase than in the ferroelectric phase. Such large values are characteristic of a highly disordered phase with large amplitude, anharmonic lattice vibrations. Along the chain axis direction the d_{001} lattice spacing is determined by the length of the covalent bonds, and therefore the thermal expansion is almost zero[20]. Thus, if one assumes the same linear thermal expansion along the *a* and *b* axes, one obtains a volumetric expansion coefficient α_V for each phase given by $\alpha_V = 2\alpha_L$. The results are given in *Table 1*. The expansion coefficients of the LTD phase, for the 60/40 copolymer, are also given and appear to be close to those of the paraelectric phase.

Similarly, the linear lattice compressibility perpendicular to the chain axis χ_L is deduced from the pressure dependence of the *d* spacing. *Table 1* again shows little difference between the three copolymers. The compressibility of the paraelectric phase is about 2.5 times larger than that of the ferroelectric phase, in agreement with its disordered nature. In addition, measurements on an oriented and polarized PVDF sample confirm an equal pressure dependence of the *a* and *b* lattice parameters.

Along the chain axis direction, the compressibility is much lower. For the homopolymer PVDF, Newman *et al.*[21] reported that $\chi_{001} = 0.015 \times 10^{-4}\ MPa^{-1}$ in the β phase and $\chi_{001} = 0.07 \times 10^{-4}\ MPa^{-1}$ in the α phase. We have used these values, as a first approximation, in determining the volumetric compressibilities χ_V of the ferroelectric and paraelectric phases of the copolymers. *Table 1* shows the results obtained using the expression $\chi_V = 2\chi_L + \chi_{001}$.

By comparing the compressibilities of these copolymers with those obtained for other crystalline polymers[22], it is clear that the compressibility of the paraelectric phase is very large and does not correspond to the general

Table 1 Linear and volumetric thermal expansion coefficients (α_L and α_V) and linear and volumetric compressibilities (χ_L and χ_V) of each crystalline phase of the three copolymers. The linear coefficients are measured perpendicular to the chain axis; the subscripts F, P and LTD stand for ferroelectric, paraelectric and low temperature disordered phase. All the values are normalized to 370 K and atmospheric pressure and correspond to the low pressure behaviour (below 150 MPa)

Parameter	80/20 copolymer	70/30 copolymer	60/40 copolymer
$10^4\ \alpha_{L,F}\ (K^{-1})$	1.1	0.9	0.9
$10^4\ \alpha_{L,P}\ (K^{-1})$	3.0	3.2	3.5
$10^4\ \alpha_{L,LTD}\ (K^{-1})$			3
$10^4\ \alpha_{V,F}\ (K^{-1})$	2.2	1.8	1.8
$10^4\ \alpha_{V,P}\ (K^{-1})$	6.0	6.4	7.0
$10^4\ \alpha_{v,LTD}\ (K^{-1})$			6
$10^4\ \chi_{L,F}\ (MPa^{-1})$	0.6	0.6	0.55
$10^4\ \chi_{L,P}\ (MPa^{-1})$	1.5	1.5	1.6
$10^4\ \chi_{L,LTD}\ (MPa^{-1})$			1.5
$10^4\ \chi_{V,F}\ (MPa^{-1})$	1.2	1.2	1.1
$10^4\ \chi_{V,P}\ (MPa^{-1})$	3.1	3.1	3.3
$10^4\ \chi_{v,LTD}\ (MPa^{-1})$			~3

Table 2 Summary of the important thermodynamic parameters for the ferroelectric transition upon increasing temperature at atmospheric pressure and at 200 MPa

Parameter	80/20 copolymer	70/30 copolymer	60/40 copolymer
	Atmospheric pressure		
T_C[a] (K)	404	362	338.5
dT_{C+}/dP[b] (K MPa^{-1})	0.32	0.38	0.31
$\Delta V/V$[c] (%)	10	6.7	–
ΔH[d] (J g^{-1})	65	33	–
ΔS[e] (J g^{-1} K^{-1})	0.16	0.09	–
	200 MPa		
T_C (K)	467.5	430	397
dT_{C+}/dP (K MPa^{-1})	0.27	0.25	0.31
$\Delta V/V$ (%)	9.9	6.6	1.5
ΔH (J g^{-1})	87	57	10
ΔS (J g^{-1} K^{-1})	0.19	0.13	0.025

[a] Curie temperature
[b] Curie temperature change with pressure
[c] Relative volume change at the Curie temperature
[d] Enthalpy change of the crystalline phase at the transition
[e] Entropy change of the crystalline phase at the transition

behaviour. Such high values are only observed for the disordered phases II and IV of poly(tetrafluoroethylene) (PTFE) (1.89×10^{-4} MPa^{-1} and 2.5×10^{-4} MPa^{-1}, respectively).

Moreover, for the paraelectric phase, the d spacing is actually non-linear and should be represented by a second-order polynomial. The second-order terms are -1.1×10^{-7} MPa^{-2} and -1.2×10^{-7} MPa^{-2}, respectively, for the 80/20 and 60/40 mol% copolymers. These values are also larger than those of most other polymers and are comparable only with those of PTFE[22].

An important result which is clearly visible from *Figure 19* is that the paraelectric d spacing changes little with composition, while the ferroelectric d spacing increases drastically with increasing TrFE content. Therefore the discontinuous change of the unit cell volume at the Curie temperature (T_C), which amounts to 10% in the 80/20 copolymer, drops to 6.7% for the 70/30 copolymer (*Table 2*). This means that the first-order character of the ferroelectric transition decreases when increasing the TrFE content. Correspondingly, the thermal hysteresis of the transition and the temperature range of phase coexistence decrease – two effects which are clearly related to the nucleation and growth of the new phase in a matrix of different volume. It is also worth noting that the volume change at T_C is insensitive to hydrostatic pressure, while the transition temperature increases rapidly with pressure.

These two results can be analysed using the Clausius–Clapeyron relation

$$\frac{dT_C}{dP} = T_C \frac{\Delta V}{\Delta H}$$

which allows the enthalpy change of the crystalline phase ΔH (and the entropy change $\Delta S = \Delta H/T_C$) to be calculated at the transition temperature, using the phase diagrams of *Figures 6*, *10* and *18*. The results obtained upon heating, at atmospheric pressure and at 200 MPa, are given in *Table 2*. They show a significant increase in ΔH (and ΔS) with increasing pressure (from $\Delta H = 33$ J g^{-1} to $\Delta H = 57$ J g^{-1} for the 70/30 copolymer in the pressure range 0.1 to 200 MPa). Furthermore, a large drop in the enthalpy and entropy changes is observed when increasing the TrFE content.

In analysing the effect of pressure on the enthalpy change, one must consider that the enthalpy H of a crystal is given by $H = U + PV$, where U is the internal energy, P is the external pressure and V is the volume. Thus, the enthalpy change at the transition can be expressed as $\Delta H = (U_{para} - U_{ferro}) + P(V_{para} - V_{ferro})$. At atmospheric pressure, the second term is negligible (around 5×10^{-3} J g^{-1}). However, at high pressures, this term is partly responsible for the enthalpy increase. For example, at 200 MPa $P(V_{para} - V_{ferro}) = 10.5$ J g^{-1} for the 80/20 copolymer, 6.9 J g^{-1} for the 70/30 copolymer and 0.9 J g^{-1} for the 60/40 copolymer. These values are not, however, sufficient to account for the increase in the enthalpy change ΔH under pressure. This means that the change in the internal energy $U_{para} - U_{ferro}$, which corresponds to the entropy change at constant volume, also increases with inreasing pressure. In fact, from *Table 2* it appears that the whole entropy change $\Delta S = S_{para} - S_{ferro}$ also increases with pressure. As an increase in the entropy of the paraelectric phase with pressure seems physically unreasonable, one must conclude that it is the entropy of the ferroelectric phase which decreases with increasing pressure.

Let us remark here that a statistical analysis of the conformationally disordered paraelectric phase[23] gives a conformational entropy of the order of $R \ln 2$, i.e. 0.084 J g^{-1} K^{-1}. This value corresponds to the increase in entropy, at constant volume, from a ferroelectric phase without conformational disorder. Thus, a comparison with the results of *Table 2* reveals both the increase in ΔS associated with the volume change at T_C and the decrease in ΔS owing to the partial disorder of the ferroelectric phase.

Indeed, an analysis of the composition effect shows that both ΔH and ΔS decrease with increasing quantities of TrFE. From an entropic point of view, this implies an increase in the ferroelectric entropy, a result in agreement with the observation of increasing disorder in the ferroelectric structure, which becomes metastable with respect to the LTD phase for the 60/40 mol% copolymer[15].

CONCLUSION

In the present paper we have described the structural properties of the ferroelectric and paraelectric crystalline phases of the P(VDF–TrFE) copolymers.

From neutron diffraction measurements as a function of temperature and pressure, we have been able to determine the thermodynamic parameters characteristic of the crystalline phases alone, of their structural phase transitions and of their melting. The results obtained at atmospheric pressure and at high pressure for three copolymers allow us to conclude that the structure and the entropy of the ferroelectric phase are much more influenced by the composition and by the external pressure than those of the paraelectric phase. The increase in the TrFE content is then equivalent to a negative pressure, as it produces an expansion of the ferroelectric unit cell and an increase in the entropy of the ferroelectric structure. This increasing disorder amplifies the effect of decreasing dipolar energy in the lowering of the Curie temperature.

The analysis of the ferroelectric transition with pressure and composition reveals that the ferroelectric transition is observed without mixing with other transitions only for TrFE contents greater than 20% and lower than 40%.

Indeed, for the 80/20 copolymer, the temperature domain of stability for the paraelectric phase decreases under pressure and at 250 MPa only 70% of the crystallites undergo the ferroelectric transition prior to melting.

For the 60/40 copolymer, the ferroelectric phase coexists with a new metastable phase which we have named the 'low temperature disordered' (LTD) phase. This new phase interpenetrates the ferroelectric crystallites, producing a distortion of the ferroelectric lattice. Under pressure, the proportion of the ferroelectric phase increases at the expense of the LTD phase which almost disappears at about 300 MPa. Further structural studies of this new phase are recommended, especially to determine whether the paraelectric–LTD phase transition, which appears to be second order-like, corresponds to a symmetry breaking or to a continuous freezing without symmetry change (as observed in an orientational glass transition[24]).

ACKNOWLEDGEMENTS

We are grateful to the ILL staff for technical support and especially to P. Convert, J. Pannetier, J. Torregrossa, P. Andant and L. Melesi for their kind assistance. It is a pleasure to acknowledge Professor J. Lajzerowicz for fruitful discussions. The samples were kindly supplied by Atochem, France.

REFERENCES

1 Wang, T. T., Herbert, J. M. and Glass, A. M. 'The Applications of Ferroelectric Polymers', Blackie and Son, Glasgow, 1987, p. 1
2 Legrand, J. F. *Ferroelectrics* 1989, **91**, 303
3 Bourgaux-Leonard, C., Legrand, J. F., Renault, A. and Delzenne, P. *Polymer* 1991, **32**, 597
4 Lovinger, A. J., Davis, G. T., Furukawa, T. and Broadhurst, M. G. *Macromolecules* 1982, **15**, 323
5 Tashiro, K., Takano, K., Kobayashi, M., Chatani, Y. and Tadokoro, H. *Polymer* 1984, **25**, 195
6 Ohigashi, H. *Jpn J. Appl. Phys.* 1985, **24**, 23
7 Daudin, B., Legrand, J. F. and Macchi, F. *J. Appl. Phys.* 1991, **27**, 39
8 Matsushige, K., Horiuchi, T., Taki, S. and Takemura, J. *Jpn J. Appl. Phys.* 1985, **24**, L203
9 Tagashira, K., Matsushige, K. and Takemura, T. *Rep. Prog. Polym. Phys. Jpn* 1985, **28**, 427
10 Koizumi, N., Haikawa, N. and Habuka, H. *Ferroelectrics* 1984, **57**, 99
11 Samara, G. A. *J. Polym. Sci., Polym. Phys. Edn* 1989, **27**, 39
12 Akashige, E., Taki, S., Horiuchi, T., Takemura, T. and Matsushige, K. *Rep. Prog. Polym. Phys. Jpn* 1987, **30**, 511
13 Lutringer, G., Meurer, B. and Weill, G. unpublished results, 1993
14 Moudden, A. H. and Vettier, C. *Phys. Rev. B* 1988, **38**, 9040
15 Bellet-Amalric, E. and Legrand, J. F. unpublished results, 1993
16 Bevington, P. R. 'Data Reduction and Error Analysis for the Physical Sciences', McGraw-Hill, New York, 1969, p. 1
17 Legrand, J. F., Lajzerowicz, J., Berge, B., Delzenne, P., Macchi, F., Bourgaux, C., Wicker, A. and Kruger, J. K. *Ferroelectrics* 1988, **78**, 151
18 Yagi, T., Tatemoto, M. and Sako, J. *Polym. J.* 1980, **12**, 209
19 Lovinger, A. J., Davis, D. D., Cais, R. E. and Kometani, J. M. *Polymer* 1987, **28**, 617
20 Delzenne, P. PhD Thesis, Grenoble University, France, 1986
21 Newman, B. A., Yoon, C. H. and Pae, K. D. *J. Mater. Sci.* 1979, **14**, 2391
22 Ito, T. *Polymer* 1982, **23**, 1412
23 Amalric, E. PhD Thesis, Grenoble University, France, 1992
24 Lüty, F. and Ortiz-Lopez, J. *Phys. Rev. Lett.* 1983, **50**, 1289